

Controlled Release from Model Blend Multilayer Films Containing Mixtures of Strong and Weak Polyelectrolytes

Yeongseon Jang,[†] Bulent Akgun,^{‡,§} Hosub Kim,[†] Sushil Satija,[‡] and Kookheon Char^{*,†}

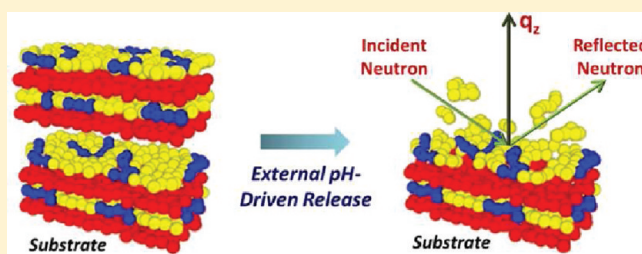
[†]The National Creative Research Initiative Center for Intelligent Hybrids, The WCU Program of Chemical Convergence for Energy & Environment, School of Chemical & Biological Engineering, Seoul National University, Seoul 151-744, Korea

[‡]NIST Center for Neutron Research, NIST, Gaithersburg, Maryland 20899-6102, United States

[§]Department of Materials Science and Engineering, University of Maryland, College Park, Maryland 20742, United States

S Supporting Information

ABSTRACT: We have designed the controlled release platforms based on polyelectrolyte (PE) blend multilayer films to investigate the release mode and kinetics at the nanoscale level. The model blend multilayer films are composed of positively charged layers with weak polyelectrolytes (PEs) (linear poly(ethylenimine), LPEI) and negatively charged blend layers with mixtures of strong (poly(sodium 4-styrenesulfonic acid), PSS) and weak (poly(methacrylic acid), PMAA) PEs. The blend multilayer films ([LPEI/PSS:PMAA]_n) with well-defined internal structure were prepared by the spin-assisted layer-by-layer (LbL) deposition method. Release properties of the multilayer films were systematically studied as a function of blend ratio by neutron reflectivity (NR), ellipsometer, AFM, FT-IR spectroscopy, and quartz crystal microbalance with dissipation (QCM-D). Since PSS strong PEs serve as robust skeletons within the multilayer films independent of external pH variation, the burst disruption of pure weak PE multilayer films was dramatically suppressed, and the release kinetics could be accurately controlled by simply changing the PSS content within the blend films. These release properties of blend multilayer films form the basis for designing the controlled release of target active materials from surfaces.



INTRODUCTION

Great efforts have been devoted to develop thin film platforms for diverse biomedical applications. In particular, thin films which provide the controlled release of active biomolecules from the surfaces have the potentials to be used as bioactive coatings on implants. Among various techniques to prepare well-designed thin films, the layer-by-layer (LbL) deposition method has received great attention due to its versatility, biocompatible processing in aqueous environment, and the ability to insert therapeutic biomolecules at a desired position within the multilayer thin film. Moreover, the LbL deposition technique facilitates the programming of the release sequence of active materials by adjusting the molecular interactions between layers.^{1–7}

Various types of multilayer thin films have been investigated for the controlled release by tuning diverse parameters including intrinsically degradable properties of polymers employed as well as external stimuli such as ionic strength, temperature, light, enzyme, electrical signal, and pH.^{8–17} Particularly for pH-responsive release systems, multilayer films containing weak polyelectrolyte (PE) pairs have been exploited because the swelling and decomposition of multilayer films can easily be controlled by changing the solution pH. Most research on the weak PE multilayer films for biological applications has been focused on the structural change of the films at specific pH 7.4, the physiological condition in blood.^{8,9}

However, multilayer films solely composed of weak PEs show rapid morphological change within 20 min and subsequent disassembly when they are exposed to low pH solution ($1 \leq \text{pH} \leq 3$).^{18,19} This rapid transition in the stability of weak PE multilayer films under acidic condition still remains as a critical obstacle for biomedical applications because pH in human body widely varies from 1.0 to 8.5.²⁰ Since most of drugs are rapidly degraded at pH 2, many material scientists and pharmacologists have focused on the design of controlled release systems to provide adequate release in gastric environment ($\text{pH} \leq 2$).^{21–23}

To overcome the film instability of weak PE multilayers in extreme pH conditions, blended solutions consisting of both weak and strong PEs can be used by taking advantage of pH-independent characteristic of strong PEs.²⁴ The PE blend multilayer films generally offer versatility to control physical and biochemical properties such as film thickness, morphology, composition, and film stability for diverse potential applications.^{25,26} In addition, the LbL deposition with blend solutions enables to insert expensive bioactive molecules effectively at a desired position and to release them in a controlled manner.⁹

However, the fundamental investigation on the internal rearrangement or the release of target molecules incorporated

Received: February 7, 2012

Revised: March 27, 2012

Published: April 3, 2012

within blend multilayer films has so far not been well understood because of the difficulty in detecting the change in internal film structure at the nanometer scale. One of useful tools for evaluating the structure of layers within a multilayer thin film is X-ray reflectivity (XRR) or neutron reflectivity (NR). Since the XRR is sensitive to electron density difference while NR is sensitive to the difference in coherent scattering length density (SLD), NR is more advantageous for the investigation of buried structure and interfacial roughness in polymer multilayer films which has a weak electron density contrast between layers. The strong neutron scattering contrast between different isotopes of hydrogen and deuterium is exploited to inscribe layering features of interest within a PE multilayer film.^{27,28}

Herein, we report the release behavior of PE chains from model blend multilayer films containing mixtures of strong and weak anionic PEs (i.e., poly(sodium 4-styrenesulfonate) (PSS) and poly(methacrylic acid) (PMAA)). PSS is a strong anionic PE, which is always fully charged independent of pH of the solutions, whereas PMAA is a weak anionic PE and its charge density varies by the solution pH. Linear poly(ethylenimine) (LPEI) is used for weak cationic PE layers. The blend multilayer films ([LPEI/PSS:PMAA]_n) with well-defined internal structure are prepared by the spin-assisted layer-by-layer (LbL) deposition method,^{29,30} and the release behavior of weak deuterated PMAA (*d*-PMAA) is systematically characterized by NR. Regularly spaced *d*-PMAA layers result in equally spaced peaks in SLD profiles, and the changes in peak shape and position after post-treatment give the ability to monitor internal rearrangement of model blend film using NR. In addition to NR measurements, changes in thickness, surface morphology, and film composition were thoroughly investigated as a function of blend ratio when the blend films were post-treated at pH 2 using ellipsometry, atomic force microscopy (AFM), and FT-IR. The *in situ* release kinetics of the model blend films were analyzed by quartz crystal microbalance with dissipation (QCM-D) measurements, providing insightful information relevant to the changes in film mass with nanogram unit.³¹ The approaches taken in the present study represent the controlled release platforms based on blend multilayer films to overcome the weakness of pH-sensitive weak PE films in acidic environment. Furthermore, the results shown here would give some insights into the improved release property of target active macromolecules from blend multilayer thin films, offering versatile, adjustable stimulative polymeric release platforms.

■ EXPERIMENTAL SECTION

Materials. Linear poly(ethylenimine) (LPEI, $M_w = 25\,000$ g/mol) and poly(methacrylic acid) (PMAA, $M_w = 15\,000$ g/mol) were purchased from Polysciences.³² Poly(sodium 4-styrenesulfonate) (PSS, $M_w = 70\,000$ g/mol) and deuterated poly(methacrylic acid) (*d*-PMAA, $M_w = 43\,000$ g/mol) were obtained from Aldrich³² and Polymer Source,³² respectively. All polymers were used as received. Silicon wafers, CaF₂ round crystal windows (Sigma-Aldrich³²), and Au sensor crystals (Q-Sense³²) were used as substrates to build blend multilayer films for further characterization.

Fabrication of Blend Multilayer Films. A LPEI solution and mixed solutions of PSS and PMAA were chosen for cationic and anionic polyelectrolyte solutions to prepare blend multilayer films. All the polymer solutions were prepared by dissolving polymers in 18 MΩ Milli-Q water with concentrations of 0.01 M (based on repeat units), and solution pH was adjusted to pH 5.0 by adding diluted HCl or NaOH solution. The blend ratio of the polyanion mixtures was varied

based on the molarity of each polymer (i.e., PSS (M):PMAA (M) = 0:100, 10:90, 30:70, 100:0). Prior to multilayer deposition, all the substrates were cleaned with piranha solution (mixtures of 70 vol % H₂SO₄ and 30 vol % H₂O₂) for 20 min at room temperature and washed thoroughly with DI water, followed by drying under nitrogen stream. The blend multilayer films, [LPEI/PSS_x:PMAA_{100-x}]_n (*x*: mole % of PSS in an anionic PE solution, *n*: number of bilayers), were prepared by the spin-assisted layer-by-layer (LbL) deposition method with a spin rate of 4000 rpm for 40 s for each deposition, followed by three consecutive washing steps for each polymer deposition with pH 5.0 DI water.

Post-Treatment of Blend Multilayer Films. The post-treatment for releasing multilayer films was performed by immersing the prepared multilayer films in pH 2.0 DI water for 10 min, which was proven to provide the sufficient disruption of multilayer films solely prepared with weak polyelectrolytes (LPEI/PMAA)₁₆. The post-treated blend multilayer films were washed thoroughly with pH 2.0 water, followed by the relevant drying process under N₂ stream.

Neutron Reflectivity (NR) Measurements. The internal structures of the blend multilayer films (in-plane averaged coherent SLD profile, surface and interface roughnesses, and total film and interlayer thicknesses) were characterized by NR measurements. The NR measurements were conducted at the NG7 horizontal reflectometer at National Institute of Standards and Technology (NIST) Center for Neutron Research (NCNR) using wavelength (λ) of 0.475 nm. Angular divergence of the beam was varied through the reflectivity measurement to get a constant footprint and a relative q_z resolution ($\Delta q_z/q_z \approx 0.04$ where $q_z = 4\pi \sin \theta/\lambda$ and θ is the incident and exit angle of the beam with respect to plane of the sample. For all the samples NR data were collected up to $q_{z,\max}$ of 0.15 Å⁻¹. The NR experiments were performed in a closed chamber with CaSO₄ platelets to keep relative humidity close to zero. Samples are equilibrated in the closed chamber at least for 1 h, and then the measurements started. Previous experience with identical bilayers films showed that the 1 h is enough to reach equilibrium. Background subtraction and main beam normalization were made using the REFLPAK³³ software package provided by NIST. The structure of thin films in general cannot be determined by direct inversion of NR data to SLD profile due to the loss of phase information during the measurement. To obtain a real space depth profile first, a candidate model was chosen and the parameters (thickness, roughness, and SLD) of the model were varied using nonlinear regression until a simulated reflectivity curve calculated from the model structure using Parratt³⁴ formalism agrees sufficiently well with the experimental data. All the data were fitted using Parratt 32 and Motofit reflectivity analysis packages. Even though this is an indirect analysis method if preliminary information is obtained by other characterization techniques (e.g., AFM, XRR, and ellipsometer), thickness, roughness, and SLD of the layers in the film can be obtained with great precision.

Characterization of Blend Multilayer Films. The total film thicknesses were measured by a variable-angle multiwavelength ellipsometer (Gaertner L2W15S830, Gaertner Scientific Corp.³²), and the surface morphologies of films were obtained with atomic force microscope (AFM) (Nanoscope IIIa, Digital Instrument³²). Experimental results were reported by averaging the values of three independent measurements for film thickness and surface roughness. The changes in frequency (Δf_n) and dissipation (ΔD_n) of an Au sensor crystal (Q-Sense³²) coated with a blend multilayer film during the post-treatment were monitored by quartz crystal microbalance equipped with dissipation (QCM-D) (Q-Sense D300, Q-Sense³²). The composition of blend multilayer films was characterized with FT-IR (FT-IR-200 spectrometer, JASCO Corp.³²). The multilayer film for FT-IR measurement was prepared on a CaF₂ crystal, which is transparent to IR light.

■ RESULTS AND DISCUSSION

The controlled release platforms based on blend multilayer films, [LPEI/PSS_x:PMAA_{100-x}]_n ($x = 0, 10, 30, 100$) were prepared by the spin-assisted LbL deposition employing

electrostatic interactions. To explore the pH-induced controlled release behavior of model blend multilayer films as a function of the blend ratio of weak (PMAA) and strong (PSS) PEs, film characteristics including thickness, internal structure, surface morphology, film mass, and film compositions before and after the post-treatment at pH 2.0 were investigated and discussed in detail in the following.

Growth Behavior of Blend Multilayer Films. Several studies using dip coating have reported that LbL films containing LPEI, in particular, exhibited the exponential growth behavior with the increase in bilayer number. Exponential growth phenomenon is based on the reversible internal rearrangement of mobile polymer chains such as LPEI.^{35,36} Excess LPEI chains exhibit diffusion into the interior of a multilayer film as well as possessing chain mobility out to the film surface in each dipping process. Therefore, the dip-assisted LbL film containing LPEI shows the exponential growth behavior. However, in the case of the spin-assisted LbL deposition method, such interdiffusion behavior of LPEI chains is significantly suppressed, and the resulting films demonstrated linear growth behavior (Figure 1). The discrepancy between

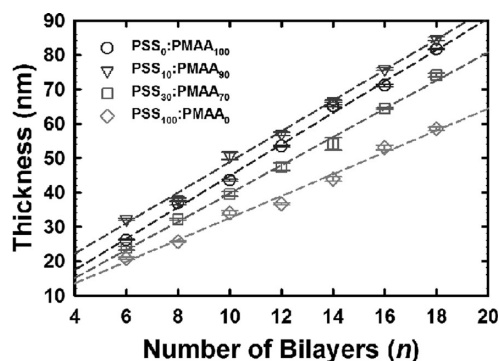


Figure 1. Thickness growth curves of blend multilayer films, $[(LPEI/PSS_x:PMAA_{100-x})_n]_{NR}$, as a function of number of bilayers. The films were assembled in pH 5.0 solutions, and thickness measurements were taken in ambient air.

conventional dip-assisted and spin-assisted LbL deposition is the different adsorption mechanisms (i.e., self-diffusion vs forced-diffusion process). The spin-assisted LbL deposition incorporates strong centrifugal force, viscous force, and air shear force along with intermolecular forces among adsorbing PE pairs.²⁹ In particular, the viscous force caused by fast solvent evaporation dramatically decreases the mobility and interdiffusion of LPEI chains within a multilayer film. Therefore, the spin-assisted LbL deposition allows us to construct a well-defined internal structure across the film thickness compared with the intermixed phase often seen in the dip-assisted LbL deposition.³⁷

The multilayers were assembled with LPEI and PSS:PMAA blend solutions at pH 5.0, which is close to pK_a values of both weak PEs. The pK_a values of LPEI and PMAA weak PEs are around 4.8–5.0 and 5.5, respectively.^{35,37} The electrostatic interactions between partially positive charges on LPEI chains and partially negative charges on PMAA chains form thick LbL-assembled multilayer films at pH 5.0 due to their coiled conformation. As has been well documented in the literature, the LbL film thickness can be controlled by simply changing the blend ratio of two anionic PEs in the adsorption solutions.^{24–26,39,40} A representative example of PE blend

multilayer films is the LbL deposition of cationic poly(allylamine hydrochloride) (PAH) solution and blended anionic solution with poly(acrylic acid) (PAA) and PSS. The relatively large thickness observed with PAH/PAA weak multilayer films is attributed to partially charged nature of PAA under the deposition conditions of pH 3.5, where PAA adsorbs in a highly coiled conformation. In contrast, a permanently negative charged PSS adopts a more stretched conformation due to higher charge per molecule and intramolecular electrostatic repulsions.²⁶ Similar to these $[PAH/PSS:PAA]_n$ blend multilayers, the decrease in the thickness growth rate of $[LPEI/PSS_x:PMAA_{100-x}]_n$ films used in the present study was observed with increasing PSS fraction in the blend solutions. Notwithstanding, the linear growth of film thickness, regardless of the blend ratio between PSS and PMAA, is highly desirable for LbL systems in many occasions, and the spin-assisted LbL deposition to grow multilayered films circumvents problems typically associated with the dip-assisted LbL deposition: the spin-assisted LbL deposition yielding well-organized internal film structure considerably facilitates the monitoring of the changes in model deuterated PE layers inserted at desired position within multilayer films using NR.

Changes in the Internal Film Structure Monitored by NR. NR experiments have been performed on model blend multilayer films to monitor the changes in internal structure before and after post-treatment. As schematically represented in Figure 2, blend multilayer films for NR study were constructed

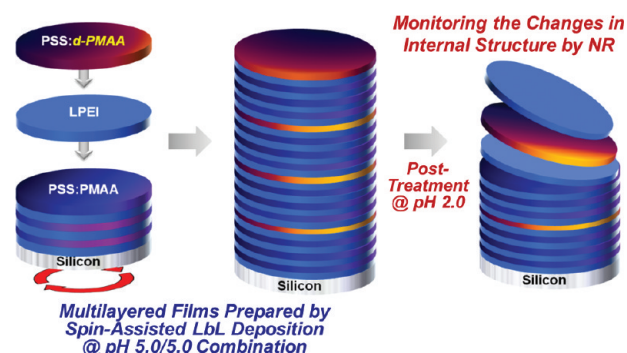


Figure 2. Schematic on the LbL deposition and post-treatment process of model blend multilayer films, $[(LPEI/PSS_x:PMAA_{100-x})_3(LPEI/PSS_x:d-PMAA_{100-x})_1]_4$, and their changes in internal structure for NR study.

by replacing PMAA with *d*-PMAA chains in the mixed polyanion solutions of PSS and PMAA in every fourth bilayer deposition to create neutron contrast. This configuration yields four spikes in the neutron SLD profile, and the changes in the height and the position of these spikes in the direction normal to the surface yield information on the diffusion and release of *d*-PMAA chains.

In order to investigate the effect of the strong PE PSS on the release behavior of weak PE *d*-PMAA chains from the multilayer films, model $[(LPEI/PSS_x:PMAA_{100-x})_3(LPEI/PSS_x:d-PMAA_{100-x})_1]_4$ multilayer films were constructed with different ratios of PSS and PMAA (i.e., PSS (M):*h*- or *d*-PMAA (M) = 0:100, 10:90, and 30:70) in blend polyanion solutions. Prior to NR measurements, the incorporated amount of PMAA within the blend multilayer films was calculated using quartz crystal microbalance (QCM) and the FT-IR measurements.²⁴ When the fraction of PSS in the blend polyanion solution is varied from 0 to 30 mol %, PSS and PMAA are incorporated

into the blend films with ratios similar to the feed ratios (Table S1 in Supporting Information). Therefore, herein, the blend ratios of PSS and PMAA in polyanion solutions can be considered as the ratios incorporated within the blended multilayer films.

Figure 3 illustrates the dramatic changes in the internal structure of multilayer films before and after the post-treatment at pH 2.0 depending on the blend ratio. The NR data were fitted with a classic box model for polyelectrolyte multilayer

films, as previously described in prior works.^{30,41–43} Each slab (protonated or deuterated layer) is characterized by SLD, thickness, and roughness in the fitting model. To fit the data, the model was constructed for an idealized LbL structure featuring sharp interfaces between adjacent layers. Initial individual layer thicknesses in the fitting model were taken from ellipsometry measurements and then adjusted to capture the Bragg peaks in the NR data. This LbL model was then modified iteratively until the reflectivity curve was best fitted to minimize χ^2 .

The entire multilayer film prepared only with weak PEs (i.e., [(LPEI/PMAA)₃(LPEI/*d*-PMAA)₁]₄) was immediately disrupted upon the acidic post-treatment at pH 2.0 (Figure 3A) due to the complete loss of electrostatic interactions between the carboxylic groups of PMAA and the secondary amine groups of LPEI. Only 4.5 nm thick layers remained on the substrate after post-treatment due to strong physical interaction of the polymer chains in the first few bilayers with the underlying substrate. Since the pK_a value of PMAA PE is around 5.5,³⁸ ionized carboxylate groups (COO⁻) in PMAA chains are protonated to their corresponding carboxylic acids (COOH) at pH 2.0, losing their negative charges that enable the association with LPEI. Subsequently, the positive charges in LPEI chains increases and the degree of ionization approaches 100% at pH 2.0 condition because the pK_a value of LPEI is approximately 4.8–5.0.³⁵ Therefore, the electrostatic interactions between negative charges on PMAA chains and positive charges on LPEI chains, which form well-ordered LbL-assembled multilayer films at pH 5.0, were significantly diminished during the post-treatment process, resulting in the precipitous disruption of the LbL film. Moreover, the disruption of the multilayer film is believed to be facilitated due to the long-ranged (inter- and intramolecular) electrostatic repulsive forces among increased positive charges of LPEI chains within the film.

However, rapid disruption of the entire multilayer film was prevented by incorporating 10% of strong PE PSS into the polyanion mixtures as well documented in Figure 3B. The multilayer film composed of [(LPEI/PSS₁₀:PMAA₉₀)₃(LPEI/PSS₁₀:*d*-PMAA₉₀)₁]₄ contains smeared Bragg peaks in the NR profile, implying that regularly spaced deuterated layers lose their neutron contrast to some extent within the film due to the mixing with protonated PE chains between the layers. The SLD profile for the blend multilayer film containing 10% PSS in Figure 3B shows that the protonated layers are more mixed with the *d*-PMAA:PSS layers in the blend film when compared with nonblend films. As a consequence of the high degree of intermixing at the substrate side of blend films, the blend multilayer film containing 10% PSS releases the weak PE *d*-PMAA from the surface, without showing the burst dissociation from the film. Since PSS chains are fully charged in aqueous solution in the pH range employed, permanent negative charges from the PSS chains are available to provide robust skeletons in blend multilayer films retaining the long-ranged electrostatic cross-linking with the positive charges of LPEI. Therefore, weak PE chains on the surface side move faster than those buried in the multilayer skeleton which is ionically cross-linked by PSS. This is consistent with the fact that the PE chains at the surface of the film has a larger diffusion coefficient than those within the film.¹⁰

Consequently, the release of weak PE PMAA from the blend multilayer films slowly transforms from the initial burst disruption to the surface attrition by increasing the amount of strong PE PSS in the mixtures of polyanions. As shown in

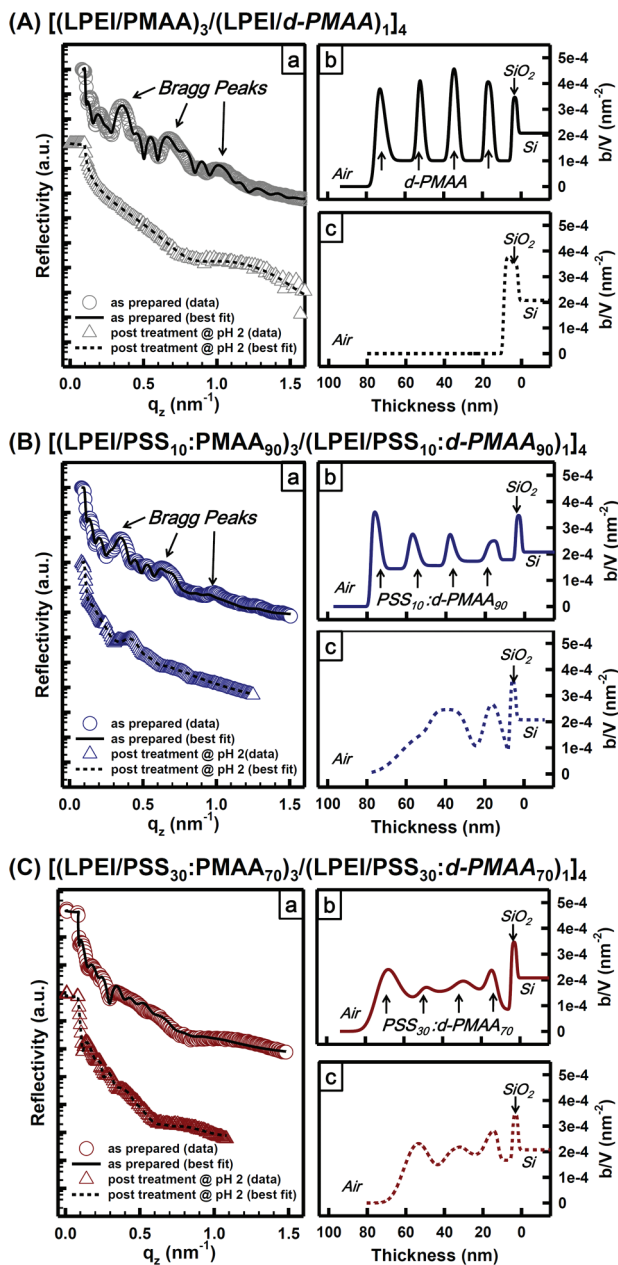


Figure 3. Neutron reflectivity (NR) curves with best fits and SLD profiles of blend multilayer films, [(LPEI/PSS:PMAA)₃(LPEI/PSS:*d*-PMAA)₁]₄. The changes in the internal structure of model multilayer films with different blend ratios of PSS:PMAA ((A) 0:100, (B) 10:90, and (C) 30:70) were monitored by NR. Films initially deposited at pH 5 are represented by circle symbols in (a) the reflectivity panels and solid lines in (b) the SLD panels while the films post-treated at pH 2 for 10 min are represented by triangle symbols in (a) the reflectivity panels and dashed lines in (c) the SLD panels.

Table 1. Film Parameters Determined from NR Measurements for Model Blend Multilayer Films with Different Blend Ratios of PSS:PMAA ((A) 0:100, (B) 10:90, and (C) 30:70) before and after Treatment at pH 2

model blend multilayer films	as-prepared films			films post-treated at pH 2		
	total film thickness (nm)	external roughness (nm)	internal roughness (nm)	total film thickness (nm)	external roughness (nm)	internal roughness (nm)
A	70.5	1.4	1.3 ± 0.5	4.5	0.6	
B	73.4	0.8	1.5 ± 0.5	40.5	8.4	4.4 ± 2.3
C	69.5	4.2	3.5 ± 0.9	56.6	4.8	2.8 ± 1.1

Figure 3C, only weak PEs residing at the top layer of the blend film are released while *d*-PMAA chains buried deep inside the blend multilayer film are virtually intact or immobile most likely due to the ionic cross-linking effect of PSS within the film even after the post-treatment, as shown in the SLD profile (NR data and the fitted SLD profile for the blend multilayer with 20% PSS show the release behavior similar to the blend multilayer containing 30% PSS (see Figure S1 in Supporting Information)).

The degree of intermixing between individual deposition layers increases with the increase of the fraction of PSS in the mixtures of polyanions. The evidence for this observation originates from the peak broadening of *d*-PMAA layers in the blend films as well as the increased SLD values of protonated LPEI layers. Another clue for the intimate intermixing mediated by PSS is found from the sharpest and highest peak of *d*-PMAA at the surface (i.e., in contact with air side), elucidating that there is no virtual interpenetration at the surface. The PSS chains embedded within the multilayer film easily capture *d*-PMAA molecules residing upper or adjacent to LPEI layers. Thus, the release of *d*-PMAA is controlled by the content of PSS in the blend multilayer film, allowing the transition from a burst disruption to the surface erosion. The controlled release behavior of blend multilayer films was also confirmed by complementary experiments with ellipsometer, AFM, QCM, and FT-IR.

Changes in Film Thickness and Surface Morphology.

The reduction in film thickness after the post-treatment was calculated as a function of the blend ratio of PSS and PMAA, based on the equation:

$$\text{thickness reduction (\%)} = \frac{t_i - t_f}{t_i} \times 100$$

where t_i and t_f are the initial as-prepared and final post-treated film thicknesses, respectively.

As shown in Figure 4, the (LPEI/PMAA)₁₆ multilayer film containing weak PMAA polyanions only is almost disassembled after the post-treatment at pH 2.0. However, the thickness reduction remarkably decreases as the PSS content is increased within the multilayer film. The reduction in film thickness estimated from the ellipsometric data coincides with the thickness measurements obtained from the fitting of NR data. Fitting of NR data yields information on film parameters including total film/interlayer thickness as well as internal/external roughness of blend multilayer films before and after post-treatment, as summarized in Table 1. (All the error bars in this paper represents ±1σ.)

Changes in surface roughness before and after the post-treatment were obtained by AFM (Figure 5A) and could also be compared with the film parameters obtained from the NR data. The surface roughness is also very important for the critical transition of surface release properties which could, in turn, be related to pore size and molecular diffusion.^{44,45} We

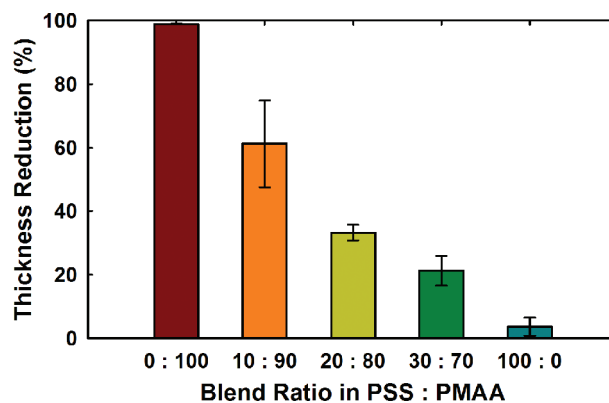


Figure 4. Thickness reduction (%) of blend multilayer films as a function of the blend ratio of PSS:PMAA polyanion mixtures, as measured by an ellipsometer.

thus quantitatively analyzed the root-mean-square (rms) surface roughness before and after the post-treatment as a function of the blend ratio (Table 1 and Figure 5B).

When a multilayer film is constructed with a pair of LPEI and PMAA, the roughness of the remaining very thin film is close to that of the Si substrate after the post-treatment because most likely the first few bilayers are conformal with the substrate. However, in the case of the blend multilayer film containing 10% PSS, some residual PEs remain with a roughened surface after the post-treatment, implying the appreciable release of polyelectrolyte chains (i.e., burst-out from the substrate but not entirely disrupted) with a small amount of PSS incorporated into the multilayer film. Consistent with the roughness values obtained by NR as well as the thickness reduction obtained from ellipsometer, the extent of surface morphological change during the pH treatment decreases as the content of PSS within the blend film is increased. We find that film stability against external pH has some correlations with the reduced change in film roughness (Figure 5B).

Release Kinetics. Release kinetics as a function of blend ratio of polyanions was monitored with *in situ* quartz crystal microbalance with dissipation (QCM-D) measurements. The relationship between frequency shift (Δf) and added or released mass per unit area (Δm) is linear, according to the Sauerbrey equation:⁴⁶

$$\Delta m = -C \frac{\Delta f_n}{n}$$

where C is the proportionality constant related to intrinsic properties of quartz ($C = 17.7 \text{ ng cm}^{-2} \text{ Hz}^{-1}$ for a 5 MHz quartz crystal) and n represents the overtone number ($n = 1, 3, 5, 7$). In addition, the dissipation change (ΔD_n), the loss of energy stored in a vibration cycle, indicates the physical characteristics of deposited layer such as viscosity, elasticity, and so forth. If ΔD_n is less than 2.0×10^{-6} and the plots of $\Delta f_n/n$

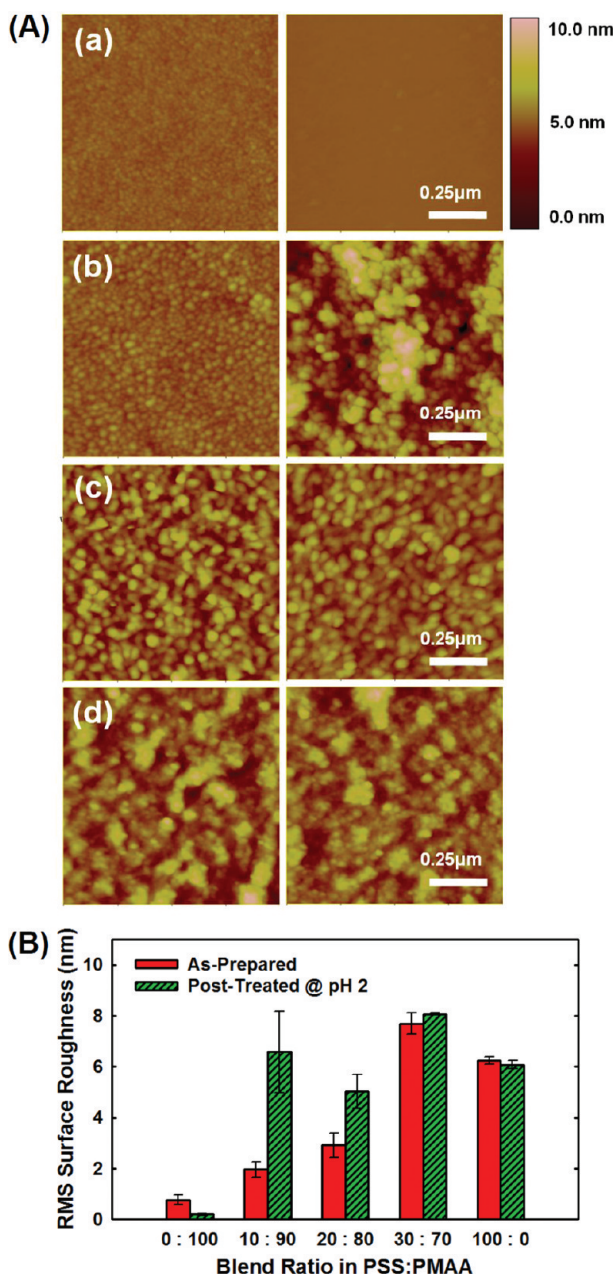


Figure 5. Changes in (A) surface morphology of as-deposited (left column) and post-treated (right column) blend multilayer films with different blend ratios of PSS:PMAA polyanions ((a) 0:100, (b) 10:90, (c) 30:70, (d) 0:100). (B) Changes in rms surface roughness as a function of blend ratio.

are superimposed with different overtones, the deposited layer has an elastic characteristic, and the physical properties such as mass and thickness of the elastic film can be estimated from the Sauerbrey equation.^{47,48} In the present study, the released film masses (ng cm^{-2}) as a function of post-treatment time at pH 2.0 were calculated based on the Sauerbrey equation because the frequency changes ($\Delta f_n/n$) were superimposed with different overtone numbers ($n = 3, 5, 7$) as well as the dissipation energy of each multilayer was less than 2.0×10^{-6} , regardless of the blend ratio (Figure S2 in Supporting Information). The released film mass curves of blend multilayer films, shown in Figure 6, were calculated from the normalized frequency changes in third overtone ($\Delta f_3/3$). Detailed

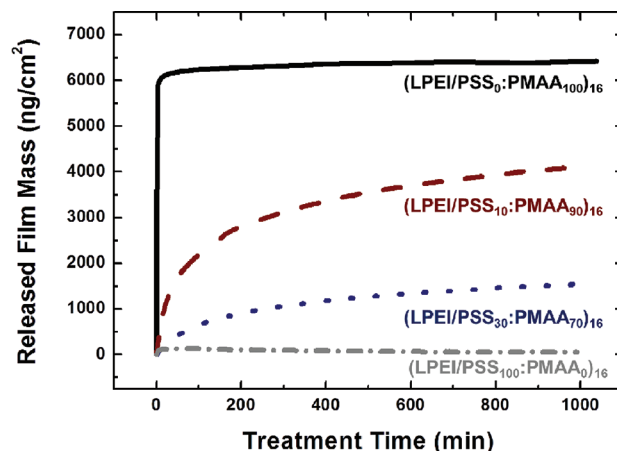


Figure 6. Release kinetics (released mass (ng/cm^2) plotted against time (min)) for blend multilayer films with different blend ratios of PSS and PMAA polyanions, monitored by QCM-D.

explanations of QCM experiments and data reduction are given in Supporting Information. As shown in Figure 6, an initial burst in the release profile of nonblended multilayer film containing LPEI and PMAA only was observed when the film is subject to post-treatment at pH 2.0, implying that the release behavior is induced directly from the substrate due to the absence of PSS. On the other hand, blended multilayer films containing 10% and 30% PSS show more retarded release rates when compared with the nonblend weak PE film. In the case of (LPEI/PSS)₁₆ multilayer film, it is clearly demonstrated that there is no change in the film mass even after the post-treatment at pH 2.0 for more than 1000 min.

The percentage of released film mass relative to the initial deposited mass was obtained from QCM measurements at different PSS blend ratios. The initial film masses were calculated using the Sauerbrey equation, based on the difference in absolute frequency (f_3) between a bare Au electrode and the electrodes coated with multilayer films. Compared with each initially deposited film mass, 81% of the original film mass is released from the multilayer film consisting of weak PEs only while 37% and 11% of masses of blended multilayer films containing 10% and 30% of PSS are lost from the film surface during the post-treatment at pH 2.0 for 1000 min. The differences in the released film masses with different strong PE contents demonstrate that the blend multilayer systems have great potential to control the amount of materials delivered as well as the rate of attrition.

Spectroscopic Changes in Film Composition. The reason why the blended films containing PSS PEs show the controlled release behavior is that the strong PSS PEs provide permanent negative charge density to associate with positive LPEI layer, and it could serve as robust skeletons of the films against external pH change. In order to verify the skeleton effect of PSS PEs within the multilayer films, independent of external pH, the composition of blend multilayer films has been analyzed with FT-IR.

Figure 7 shows the IR spectra of PSS in the blend multilayer films with different blend ratios of PSS and PMAA before (open symbols) and after (closed symbols) the post-treatment at pH 2.0 for 10 min. The FT-IR spectra of PSS shows the characteristic peak at 1035 cm^{-1} for the stretching vibration of SO_3^- groups.⁴⁸ The amount of PSS retained within the

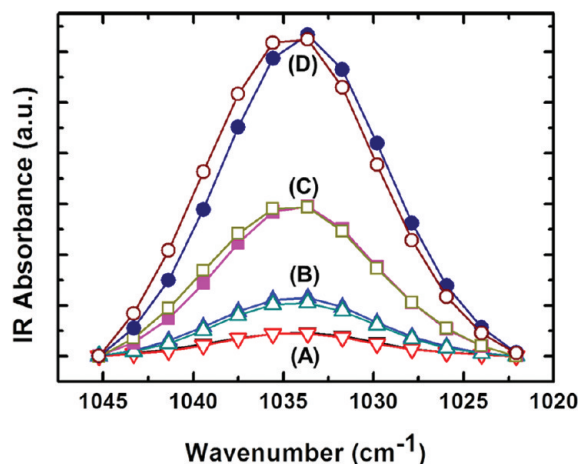


Figure 7. FT-IR spectra of PSS on the region of S=O stretching vibration of SO_3^- for as-prepared films (open symbols) and the films post-treated at pH 2 (closed symbols) with different blend ratios in PSS:PMAA polyanion mixtures ((A) ∇ , 10:90; (B) \triangle , 20:80; (C) \blacksquare , 30:70; and (D) \bullet , 100:0).

multilayer films is almost constant even after the post-treatment, regardless of the blend ratios of PSS and PMAA.

On the other hand, weak PEs shows significant differences in IR absorbance when as-prepared films were subject to the post-treatment. Figure 8 shows that as the content of PSS is increased, the degree of decrease in the IR absorbance of PMAA is reduced and also more protonated PMAA chains confirmed by a peak at 1701 cm^{-1} remain within the blend film even after treatment. These results imply that every carboxylic group in PMAA chains is protonated at pH 2.0, but the protonated PMAA chains cannot easily escape from the blend multilayer films due to strong ionic cross-linking effect of PSS PEs. The remaining amount of LPEI also increases within the films as the PSS content within the multilayer film is increased (see Figure S3 in Supporting Information). These FT-IR analyses further support that pH-independent PSS chains serve as robust skeletons to resist the total disruption of $(\text{LPEI}/\text{PMAA})_n$ weak PE multilayer films when the multilayer film is subject to treatment in acidic media. As a result, the burst disruption of multilayer films is dramatically suppressed, and the release kinetics could be finely tuned simply by varying the PSS content within the multilayer films.

CONCLUSION

A model controlled release platform triggered in acidic conditions (i.e., pH 2.0) has been developed based on blend multilayer films incorporating the mixtures of strong and weak PEs. LbL systems containing $[\text{LPEI}/\text{PSS}_x:\text{PMAA}_{100-x}]_{16}$ have been prepared by the spin-assisted deposition method, which offers well-defined internal structure with linear growth behavior. The controlled release behavior as a function of blend ratio of PSS and PMAA has been investigated in terms of the changes in internal structure as well as the release kinetics at the nanoscale level. As the incorporation ratio of PSS is increased within the blend multilayer film, the precipitous disruption of a film solely composed of weak PEs is dramatically suppressed and switches to surface erosion. The released mass and kinetics of the film could be finely tuned as a function of the blend ratio. In addition, we have elucidated that PSS PEs provide the robust skeletons within the blend multilayer films, independent of pH variation, as shown by

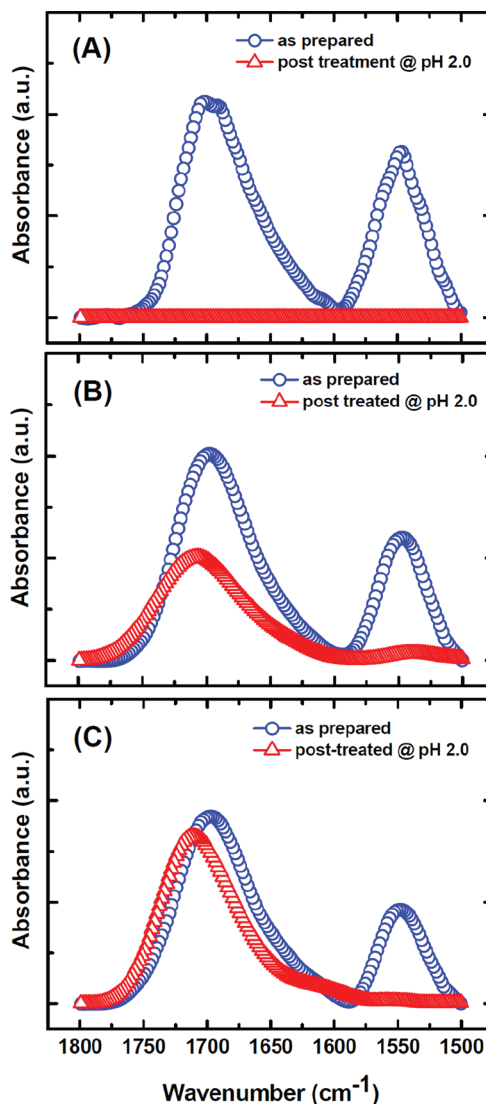


Figure 8. FT-IR absorption spectra of PMAA chains, in the regions at 1701 and 1540 cm^{-1} associated with COOH and COO^- groups for as-prepared films (circle symbols) and the films post-treated at pH 2.0 (triangle symbols) at different blend ratios in PSS:PMAA polyanion mixtures ((A) 0:100, (B) 10:90, (C) 30:70).

the comparison of the analysis of SLD profiles as well as FT-IR absorbance of model films before and after treatment. The approaches taken in the present study for the controlled release represent the improved release property of multilayer thin films. Therefore, the controlled release behavior of model blend multilayer systems triggered at low pH offers the opportunity to design versatile polymeric delivery platforms responding to external stimuli for various biomedical applications.

ASSOCIATED CONTENT

Supporting Information

Incorporation ratio of PMAA within the multilayer films (Table S1); NR curves with best fits and the SLD profiles of $[(\text{LPEI}/\text{PSS}_{20}:\text{PMAA}_{80})_3(\text{LPEI}/\text{PSS}_{20}:\text{PMAA}_{80})_1]_4$ (Figure S1); QCM raw data of model multilayer films (Figure S2); FT-IR spectra of LPEI (Figure S3) for as-prepared and post-treated samples. This material is available free of charge via the Internet at <http://pubs.acs.org>.

■ AUTHOR INFORMATION

Corresponding Author

*Tel +82-2-880-7431, fax +82-2-873-1548, e-mail khchar@plaza.snu.ac.kr.

Notes

The authors declare no competing financial interest.

■ ACKNOWLEDGMENTS

This work was financially supported by the National Research Foundation of Korea (NRF) funded by the Korea Ministry of Education, Science, and Technology (MEST) (The National Creative Research Initiative Program for "Intelligent Hybrids Research Center" (No. 2010-0018290), the Brain Korea 21 Program in SNU Chemical Engineering, and the WCU Program of Chemical Convergence for Energy and Environment (R31-10013)). Y. Jang is also grateful for the financial support from the Seoul Science Fellowship. We thank NIST Center for Neutron Research (NCNR) for assigning enough beamtime to conduct NR experiments at NG7 beamline. In addition, we appreciate Dr. Ki-Yeon Kim and Dr. Jung-Soo Lee for allowing us to use the REF-V beamline at the HANARO Center of Korea Atomic Energy Research Institute (KAERI).

■ REFERENCES

- (1) Tang, Z. Y.; Wang, Y.; Podsiadlo, P.; Kotov, N. A. *Adv. Mater.* **2006**, *18* (24), 3203–3224.
- (2) Boudou, T.; Crouzier, T.; Ren, K. F.; Blin, G.; Picart, C. *Adv. Mater.* **2010**, *22* (4), 441–467.
- (3) Jang, Y.; Park, S.; Char, K. *Korean J. Chem. Eng.* **2011**, *28* (5), 1149–1160.
- (4) Swiston, A. J.; Cheng, C.; Um, S. H.; Irvine, D. J.; Cohen, R. E.; Rubner, M. F. *Nano Lett.* **2008**, *8* (12), 4446–4453.
- (5) Wood, K. C.; Boedicker, J. Q.; Lynn, D. M.; Hammond, P. T. *Langmuir* **2005**, *21* (4), 1603–1609.
- (6) Ono, S. S.; Decher, G. *Nano Lett.* **2006**, *6* (4), 592–598.
- (7) De Geest, B. G.; Sanders, N. N.; Sukhorukov, G. B.; Demeester, J.; De Smedt, S. C. *Chem. Soc. Rev.* **2007**, *36* (4), 636–649.
- (8) Kim, B. S.; Smith, R. C.; Poon, Z.; Hammond, P. T. *Langmuir* **2009**, *25* (24), 14086–14092.
- (9) Hong, J.; Kim, B. S.; Char, K.; Hammond, P. T. *Biomacromolecules* **2011**, *12* (8), 2975–2981.
- (10) Jomaa, H. W.; Schlenoff, J. B. *Macromolecules* **2005**, *38* (20), 8473–8480.
- (11) Wong, J. E.; Gaharwar, A. K.; Muller-Schulte, D.; Bahadur, D.; Richtering, W. *J. Colloid Interface Sci.* **2008**, *324* (1–2), 47–54.
- (12) Volodkin, D. V.; Madaboosi, N.; Blacklock, J.; Skirtach, A. G.; Mohwald, H. *Langmuir* **2009**, *25* (24), 14037–14043.
- (13) Wood, K. C.; Zacharia, N. S.; Schmidt, D. J.; Wrightman, S. N.; Andaya, B. J.; Hammond, P. T. *Proc. Natl. Acad. Sci. U. S. A.* **2008**, *105* (7), 2280–2285.
- (14) Etienne, O.; Schneider, A.; Taddei, C.; Richert, L.; Schaaf, P.; Voegel, J. C.; Egles, C.; Picart, C. *Biomacromolecules* **2005**, *6* (2), 726–733.
- (15) Kharlampieva, E.; Ankner, J. F.; Rubinstein, M.; Sukhishvili, S. A. *Phys. Rev. Lett.* **2008**, *100* (12), 128303.
- (16) Jia, Y.; Fei, J.; Cui, Y.; Yang, Y.; Gao, L.; Li, J. *Chem. Commun.* **2011**, *47*, 1175–1177.
- (17) Song, W.; He, Q.; Mohwald, H.; Yang, Y.; Li, J. *J. Controlled Release* **2009**, *139*, 160–166.
- (18) Mendelsohn, J. D.; Barrett, C. J.; Chan, V. V.; Pal, A. J.; Mayes, A. M.; Rubner, M. F. *Langmuir* **2000**, *16* (11), 5017–5023.
- (19) Lutkenhaus, J. L.; McEnnis, K.; Hammond, P. T. *Macromolecules* **2008**, *41* (16), 6047–6054.
- (20) Vander, A. J.; Sherman, J. H.; Luciano, D. S. *Human Physiology: the Mechanisms of Body Function*; McGraw-Hill: New York, 1994.
- (21) Estey, T.; Kang, J.; Schwendeman, S. P.; Carpenter, J. F. *J. Pharm. Sci.* **2006**, *95* (7), 1626–1639.
- (22) Risbud, M. V.; Hardikar, A. A.; Bhat, S. V.; Bhonde, R. R. *J. Controlled Release* **2000**, *68*, 23–30.
- (23) Rao, V. M.; Engh, K.; Qiu, Y. *Int. J. Pharm.* **2003**, *252*, 81–86.
- (24) Cho, J. H.; Quinn, J. F.; Caruso, F. *J. Am. Chem. Soc.* **2004**, *126* (8), 2270–2271.
- (25) Quinn, A.; Such, G. K.; Quinn, J. F.; Caruso, F. *Adv. Funct. Mater.* **2008**, *18* (1), 17–26.
- (26) Quinn, A.; Tjipto, E.; Yu, A. M.; Gengenbach, T. R.; Caruso, F. *Langmuir* **2007**, *23* (9), 4944–4949.
- (27) Decher, G. *Science* **1997**, *277* (5330), 1232–1237.
- (28) Losche, M.; Schmitt, J.; Decher, G.; Bouwman, W. G.; Kjaer, K. *Macromolecules* **1998**, *31* (25), 8893–8906.
- (29) Cho, J.; Char, K.; Hong, J. D.; Lee, K. B. *Adv. Mater.* **2001**, *13* (14), 1076–1078.
- (30) Kharlampieva, E.; Kozlovskaya, V.; Chan, J.; Ankner, J. F.; Tsukruk, V. V. *Langmuir* **2009**, *25* (24), 14017–14024.
- (31) Turon, X.; Rojas, O. J.; Deinhammer, R. S. *Langmuir* **2008**, *24* (8), 3880–3887.
- (32) Commercial materials, instruments and equipment are identified in this paper in order to specify the experimental procedure as completely as possible. In no case does such identification imply a recommendation or endorsement by the National Institute of Standards and Technology nor does it imply that the materials, instruments, or equipment identified are necessarily best available for the purpose.
- (33) Kienzle, P. A.; O'Donovan, K. V.; Ankner, J. F.; Berk, N. F.; Majkrzak, C. F. <http://www.ncnr.nist.gov/reflpak>, 2000–2006.
- (34) Parratt, L. G. *Phys. Rev.* **1954**, *95* (2), 359–369.
- (35) Yoo, P. J.; Zacharia, N. S.; Doh, J.; Nam, K. T.; Belcher, A. M.; Hammond, P. T. *ACS Nano* **2008**, *2* (3), 561–571.
- (36) Yoo, P. J.; Nam, K. T.; Qi, J. F.; Lee, S. K.; Park, J.; Belcher, A. M.; Hammond, P. T. *Nat. Mater.* **2006**, *5* (3), 234–240.
- (37) Lee, Y. M.; Park, D. K.; Choe, W. S.; Cho, S. M.; Han, G. Y.; Park, J.; Yoo, P. J. *J. Nanosci. Nanotechnol.* **2009**, *9* (12), 7467–7472.
- (38) Chao, G. T.; Deng, H. X.; Huang, Q.; Jia, W. J.; Huang, W. X.; Gu, Y. C.; Tan, H. P.; Fan, L. Y.; Liu, C. B.; Huang, A. L.; Lei, K.; Gong, C. Y.; Tu, M. J.; Qian, Z. Y. *J. Polym. Res.* **2006**, *13* (5), 349–355.
- (39) Hubsch, E.; Ball, V.; Senger, B.; Decher, G.; Voegel, J. C.; Schaaf, P. *Langmuir* **2004**, *20* (5), 1980–1985.
- (40) Sui, Z. J.; Schlenoff, J. B. *Langmuir* **2004**, *20* (14), 6026–6031.
- (41) Hiller, J.; Rubner, M. F. *Macromolecules* **2003**, *36* (11), 4078–4083.
- (42) Kharlampieva, E.; Kozlovskaya, V.; Ankner, J. F.; Sukhishvili, S. A. *Langmuir* **2008**, *24* (20), 11346–11349.
- (43) Fredin, N. J.; Zhang, J.; Lynn, D. *Langmuir* **2005**, *21*, 5801–5811.
- (44) Quinn, J.; Caruso, F. *Langmuir* **2004**, *20*, 20–22.
- (45) Felix, O.; Zheng, Z. Q.; Cousin, F.; Decher, G. *C. R. Chim.* **2009**, *12* (1–2), 225–234.
- (46) Sauerbrey, G. *Z. Phys.* **1959**, *155* (2), 206–222.
- (47) Vogt, B. D.; Lin, E. K.; Wu, W. L.; White, C. C. *J. Phys. Chem. B* **2004**, *108* (34), 12685–12690.
- (48) Lee, H.-S.; Eckmann, D. M.; Lee, D.; Hickok, N. J.; Composto, R. J. *Langmuir* **2011**, *27* (20), 12458–12465.
- (49) Kuo, C.-W.; Wen, T.-C. *Eur. Polym. J.* **2008**, *44* (11), 3393–3401.